Chinese Chemical Letters 37 (2026) 111526

Contents lists available at ScienceDirect

Chinese Chemical Letters

journal homepage: www.elsevier.com/locate/cclet

Chinese medicine residue-derived biochars for peracetic acid activation in sulfamethoxazole removal *via* non-radical pathways

Chenghuan Qiao[1], Yaohua Wu[1], Yihong Chen, Chuchu Chen, Juanshan Du, Wenrui Jia, Yongqi Liang, Qinglian Wu, Huazhe Wang*, Wan-Qian Guo

State Key Laboratory of Urban-rural Water Resource and Environment, Harbin Institute of Technology, Harbin 150090, China

ARTICLE INFO

Article history:
Received 21 December 2024
Revised 6 May 2025
Accepted 1 July 2025
Available online 2 July 2025

Keywords:
Peracetic acid
Chinese medicine residues
Biochar
Electron transfer process
Sulfamethoxazole

ABSTRACT

According to the "New Coronavirus Pneumonia (COVID-19) Tenth Edition Diagnosis and Treatment Plan", residues from three prescriptions including Qingfei-Paidu Formula, Huashi-Baidu Formula, and Xuanfei-Zhixue Formula were selected as precursors for biochar preparation. The resulting Chinese medicine residue-derived biochars (CMR-BCs), prepared using different prescriptions and pyrolysis temperatures, were used to activate peracetic acid (PAA) for sulfamethoxazole (SMX) removal. Biochar (q800) produced from 800 °C-treated Qingfei-Paidu Formula residue achieved ~60 % SMX adsorption removal efficiency, outperforming other CMR-BCs. All prepared CMR-BC samples demonstrated oxidative degradation of SMX via activating PAA, with efficiencies ranging from ~20.8 % to 45.5 %, which might be ascribed to their abundant oxygen-containing functional groups and graphitic structures. Electro-chemical analysis and quenching tests indicated that the direct electron-transfer (DET) process was identified as the primary non-radical degradation mechanism. The formation of CMR-BCs-PAA* interfacial complexes enhanced the overall oxidation potential, facilitating the redox reaction between CMR-BCs-PAA* and SMX. In total, this study offers new insights into the non-radical mechanism of CMR-BC/PAA systems, presenting a potential solution for the resource utilization of Chinese medicine residue wastes.

© 2025 Published by Elsevier B.V. on behalf of Chinese Chemical Society and Institute of Materia Medica, Chinese Academy of Medical Sciences.

Advanced oxidation processes (AOPs) involved in strong oxidants such as hydrogen peroxide, persulfates, chlorine, and peracetic acid (PAA), in which PAA has garnered considerable attention due to its high redox potential ($E_0 = 1.96$ V) and the low toxicity of its byproducts [1–3]. PAA can be activated using ultraviolet (UV) irradiation, metal ions, or carbon-based catalysts to generate reactive radicals, including hydroxyl radicals (•OH), acetoxy radicals (CH_3CO_2•), and acetyl peroxy radicals (CH_3CO_3•) [4–6]. For instance, medium-pressure UV activation of PAA produces •OH and CH_3CO_3•, facilitating the degradation of norfloxacin [7]. Co(II) activation of PAA generates CH_3CO_2• and CH_3CO_3• without forming •OH [8]. Activated carbon fibers (ACFs) have also been used to catalyze PAA, where the generated •OH and CH_3CO_2• efficiently degrade dyes [9]. Recent researches emphasized the non-radical direct electron transfer (DET) processes in the interaction of oxidants (*e.g.*, persulfates and periodate) and carbon-based catalysts (*e.g.*, carbon nanotubes, graphene oxide, and biochar) [10–12]. For example, surface complexation was occurred between carbon-based materials and PAA, elucidating the contribution of non-radical DET mechanisms in improving contaminant degradation [13,14]. Recently, biochar has also been used for the activation of PAA. Zhou *et al.* [15] reported that sludge-derived biochar (SDBC) activated PAA through both radical and non-radical pathways to degrade fluoroquinolone antibiotics. In this case, iron species in SDBC generated organic radicals, while the carbon composition facilitated non-radical pathways.

The conversion from residues into biochar is an effective method for resource recycling. In recent years, residues such as sludge [15], food waste [16], livestock manure [17]. have been transformed into biochar. Traditional Chinese medicine residue (CMR), a common agricultural waste with a complex and stable structure, poses environmental and ecological risks due to its high treatment costs [18,19]. Although biological fermentation is the primary method for CMR treatment, it produces low-value products that limit broader applications [4,20,21]. CMR, however, is a promising biochar precursor due to its high carbon content and abundant components such as cellulose, hemicellulose, lignin, and microelements (*e.g.*, calcium, phosphorus, and iron) [22]. Existing research on Chinese medicine residue-derived biochars (CMR-BCs)

* Corresponding author.
E-mail address: huazhewang@hit.edu.cn (H. Wang).
[1] These authors contributed equally to this work.

https://doi.org/10.1016/j.cclet.2025.111526
1001-8417/© 2025 Published by Elsevier B.V. on behalf of Chinese Chemical Society and Institute of Materia Medica, Chinese Academy of Medical Sciences.

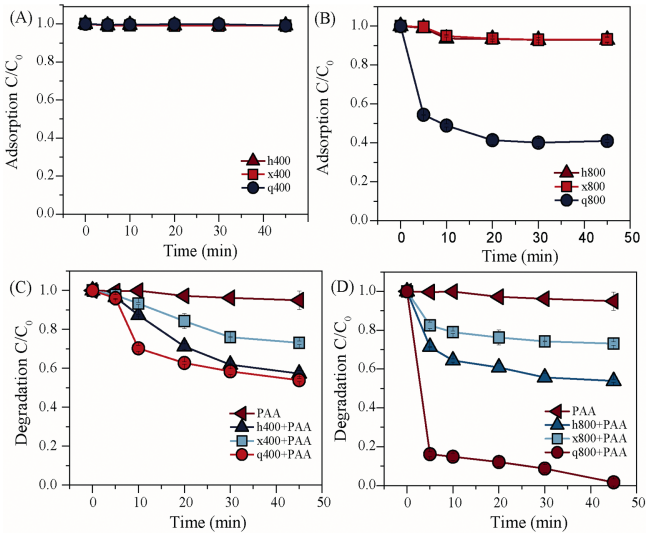


Fig. 1. The adsorption removal efficiency of SMX by (A) 400 °C- and (B) 800 °C- treated CMR-BCs. The catalytic degradation efficiency of SMX in different (C) 400 °C- and (D) 800 °C- treated CMR-BCs/PAA system. (C) Experimental conditions: $[h400]_0 = [x400]_0 = [q400]_0 = 2$ g/L, $[h800]_0 = [x800]_0 = [q800]_0 = 1$ g/L, $[PAA]_0 = 2$ mmol/L, $[SMX]_0 = 20$ μmol/L, pH 7.0, and $T = 25 \pm 2$ °C.

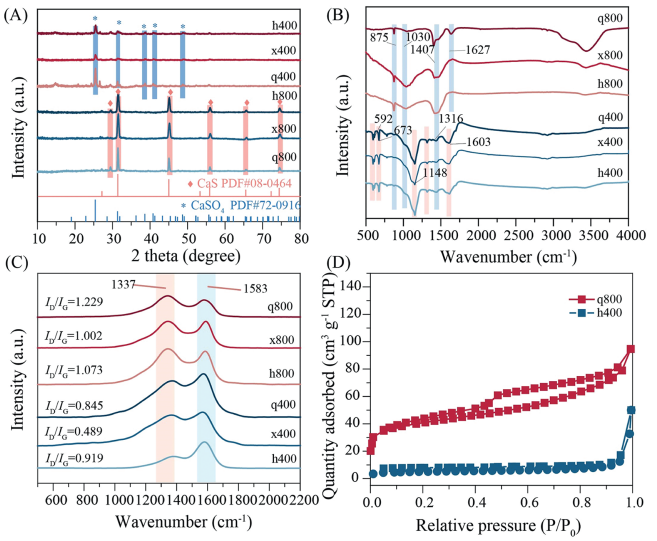


Fig. 2. (A) XRD patterns, (B) FT-IR spectra, (C) Raman spectra for different CMR-BCs. (D) N_2 adsorption/desorption isotherms for q800 and h400 samples.

has primarily focused on pollutant adsorption. However, studies investigating PAA activation *via* CMR-BCs are still limited, and there is a need to elucidate the mechanisms underlying contaminant degradation in the CMR-BCs/PAA system. Additionally, most studies to date have prepared biochar from individual Chinese medicine components without considering the broader application of Chinese medicine prescriptions. Since prescriptions consist of multiple components and are more frequently used in practice, developing biochar based on these prescriptions is a more practical and impactful approach. Therefore, transforming CMR into biochar for PAA activation provides a sustainable and efficient solution for water treatment, offering a high-value approach to agricultural waste reuse.

This study explored the preparation of biochars from three types of CMRs using simple pyrolysis at different temperatures. SMX was selected as the target contaminant to evaluate the effectiveness and mechanisms of CMR-BC in activating PAA. First, the adsorption and degradation performance of SMX in the CMR-BCs/PAA system was investigated. And then, we characterized the structure of as-prepared CMR-BCs. Furthermore, the oxidative reaction mechanism, *i.e.*, the non-radical DET process, was identified *via* radical quenching tests, electron paramagnetic resonance (EPR), and electrochemical analysis in the CMR-BCs/PAA/SMX systems. Chemicals used in this study were listed in Text S1 (Supporting information). Material preparation was described in Text S2 (Supporting information). The characterization of prepared CMR-BCs was shown in Text S3 (Supporting information). The details of adsorption and degradation experiments were described in Text S4 (Supporting information). Additionally, analytical methods were detailed in Text S5 (Supporting information).

The CMR-BCs treated at 400 °C (*i.e.*, q400, h400, and x400 samples) demonstrated negligible adsorption removal of SMX (Fig. 1A). However, the 800 °C-treated CMR-BCs (q800, h800, and x800) demonstrated higher adsorption removal efficiencies for SMX compared to their 400 °C counterparts, suggesting that higher pyrolysis temperatures enhanced the adsorption capacity of CMR-BCs (Fig. 1B). This observation aligns with the findings of Huang *et al.* [23], who reported that increasing the pyrolysis temperature of poplar biochar improved its adsorption capacity. Regarding oxidative removal, PAA alone exhibited weak direct oxidation, achieving only ~5.1 % degradation of SMX in 45 min (Fig. 1C). However, the degradation efficiencies of SMX in the 400 °C-treated CMR-BCs/PAA systems followed the order: q400 (~45.5 %) > h400 (~41.9 %) > x400 (~26.6 %), after excluding the contribution of adsorption, highlighting the catalytic activation of PAA by these biochars (Fig. 1C). Additionally, the oxidative contribution of SMX in 800 °C-treated CMR-BCs/PAA followed the order: h800 (~40.0 %) > q800 (~25.4 %) > x800 (~20.8 %) after accounting for adsorption effects (Fig. 1D). Compared to the oxidative contribution of 400 °C-treated CMR-BCs at 2 g/L, there was no significant enhancement in the oxidative degradation of SMX with 800 °C-treated CMR-BCs at 1 g/L, indicated that the higher pyrolysis temperature of CMR did not influence the activation of PAA. Therefore, despite differences in Chinese medicine prescriptions and pyrolysis temperatures, all prepared CMR-BCs exhibited catalytic activity for PAA activation. Jia *et al.* [24] found that combining ultrasound and biochar from *Acanthpanax senticosus* precursors could activate persulfate for degrading ATZ, but the reactivity of CMR-BC itself was not fully explored. To better understand the influence of pyrolysis temperature and precursor formulations on SMX removal in the CMR-BCs/PAA system, additional characterization of the CMR-BCs was conducted.

The X-ray diffraction (XRD) analysis of the 400 °C-treated samples reveal distinct diffraction peaks at 28.5°, 31.9°, 38.6°, and 41.3°, corresponding to the (002), (211), (202), and (031) lattice planes of $CaSO_4$ (PDF #72–0916) (Fig. 2A). In contrast, the 800 °C-treated samples exhibit peaks at 2θ values of 31.3°, 44.9°, and 55.8°, indexed to the (200), (220), and (222) planes of CaS (PDF #08–0464) (Fig. 2A). These findings suggest that $CaSO_4$ in the 400 °C-treated CMR-BCs was reduced by carbon to form CaS under higher pyrolysis temperatures (~800 °C). The presence of $CaSO_4$ or CaS in the CMR-BCs likely originated from the Chinese medicine prescriptions. However, the broad peak typically associated with carbon was suppressed, likely due to its low crystallinity, consistent with prior studies on CaS-loaded biochar [25]. Despite the presence of CaS in all 800 °C-treated CMR-BCs, their SMX adsorption capacities varied, indicating that $CaSO_4$ or CaS composition is not the primary factor influencing SMX adsorption.

FTIR spectra were applied to investigate the functional groups of CMR-BCs in Fig. 2B. The enhanced peaks of 800 °C-treated CMR-BCs at 875 cm^{-1} (C–H) and 1407 cm^{-1} (-COOH) compared to their

400 °C-treated counterparts suggest a potential impact on adsorption capacity. Peaks at 592, 669, 1143, and 1608 cm^{-1}, attributed to $CaSO_4$, were observed in the 400 °C-treated samples, consistent with the XRD results. However, the characteristic peaks of CaS lie outside the mid-infrared region, which cannot be observed in the 800 °C-treated CMR-BCs [26]. Additionally, the q800 sample exhibited H–O-H bending at 1627 cm^{-1} and ν(O–H) bands at ~3400 cm^{-1}, reflecting its higher water content [27]. Raman spectra (Fig. 2C) revealed two broad peaks at ~1340 cm^{-1} and ~1590 cm^{-1}, corresponding to the D and G bands, respectively. The intensity ratio of these bands (I_D/I_G) indicates the defect level. The q800 sample exhibited the highest I_D/I_G ratio (~1.229) among the samples, indicating a higher degree of graphitic carbon defects [28]. These defects, associated with functional groups such as carbonyl, hydroxyl, and epoxy, enhance the adsorption and catalytic oxidation of organic pollutants [29,30]. Consequently, the superior SMX removal efficiency of the q800 sample may be attributed to its higher defect density in graphitic carbon.

The BET surface area and pore size distribution play crucial roles in determining the surface adsorption capacity of materials. Fig. 2D shows that the N_2 adsorption/desorption isotherm of the q800 sample corresponds to a type IV isotherm with a type H4 hysteresis loop, indicating an irregular pore structure. However, the h400 sample exhibits a type III isotherm, suggesting weak interactions between the adsorbate and N_2 [31]. The order of BET surface area is as follows: q800 (145.588 m^2/g) > h800 (116.546 m^2/g) > x800 (27.071 m^2/g) > h400 (18.366 m^2/g) > q400 (13.627 m^2/g) > x400 (4.936 m^2/g), aligning with the SMX adsorption removal efficiencies (Table S1 in Supporting information). The pore size distribution curves reveal a hierarchically mesoporous structure in the prepared CMR-BCs, with pores in the q800 sample centered around 6.1 nm (Fig. S1 in Supporting information). The enhanced pore structure in the q800 sample can be attributed to graphitization and the volatilization of organic components during high-temperature treatment [32]. Elemental analysis of the h400 and q800 samples confirm the presence of C, O, Ca, and S (Figs. S2A and B in Supporting information). In the C 1s spectra of h400 and q800 samples, four typical peaks are located at around 284.5, 285.4, 288.0, and 292.8 eV, corresponding to C–C/C=C, C–O, C=O, and π-π^* shake up (Figs. S3A and C in Supporting information), respectively [33]. The q800 sample contains a higher percentage of oxygen-containing functional groups (36.64 %) compared to the h400 sample (23.33 %), consistent with the Raman results. The π-π^* shake-up fraction was determined to be 8.54 % and 4.7 % in both q800 and h400 samples, respectively, reflecting their graphitic structures [34]. It is noted that the π-π^* shake-up fraction disappeared after the reaction, indicating the significant role of graphitic structures in activating PAA or SMX adsorption (Fig. S4 in Supporting information). Based on the characterization results, the CaS/$CaSO_4$ composition or surface area were not the primary factors that affecting the adsorption performance of prepared CMR-BCs. Meanwhile, the electron-rich oxygen-containing functional groups (C–O and C=O) and graphitic carbon structures in the CMR-NCs played a crucial role in PAA activation [35].

In order to investigate the effects of different pyrolysis temperatures and precursor prescriptions of CMR-BCs on the PAA activation for degrading SMX, the q800 sample, with the highest SMX removal efficiency, and the h400 sample, with a relatively high oxidative contribution to SMX removal, were chosen for this purpose. Methanol (MeOH), a quencher of •OH and organic radicals due to its high reaction rate constants, shows negligible impact on SMX degradation in both systems (Figs. 3A and B). This suggested that •OH and $CH_3C(O)OO^•$ are not significant contributors to the CMR-BCs/PAA system. EPR analysis further supported this conclusion. No DMPO-•OH adduct signal was detected in the PAA alone, PAA/SMX, h400/PAA, or h400/PAA/SMX systems (Fig. S5 in Supporting information). In the q800/PAA system, a DMPO-•OH signal was observed, but its intensity remained unaffected by the presence of SMX, confirming that •OH does not play a role in SMX degradation (Fig. 3C). *Tert*–butyl alcohol (TBA) inhibited SMX removal, likely due to its interaction with the carbon surface, which may hinder DET process [28]. Consequently, radicals are ruled out as contributors to SMX degradation. Previous studies have shown singlet oxygen ($^1O_2$) to be reactive species in degrading organic contaminants [36,37]. Sodium azide (NaN_3), a common $^1O_2$ scavenger with a high second-order reaction rate (~1×10^9 L mol^{-1} s^{-1}), was excessively introduced into the CMR-BCs-PAA reaction systems [38]. The addition of NaN_3 caused an obvious inhibitory effect in both the h400/PAA and q800/PAA systems, indicating that $^1O_2$ can play a significant role in the degradation of SMX. However, quenching experiments alone are insufficient to confirm the mechanism. NaN_3 can also act as an electron acceptor, potentially disrupting DET processes [39]. We then further verified the role of $^1O_2$ by EPR tests using TEMP as a capture agent. As shown in Fig. 3D, PAA self-decomposition generated $^1O_2$, while no $^1O_2$ signal was observed in the q800/PAA or q800/PAA/SMX systems. This suggested that q800 complexed with PAA at the interface, initiating DET processes rather than generating $^1O_2$.

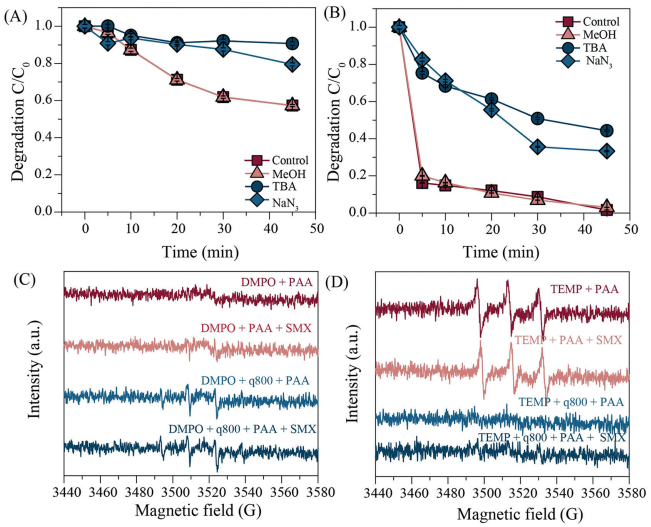


Fig. 3. SMX removal under different quenching conditions in (A) h400/PAA and (B) q800/PAA systems. (C) EPR signals in different systems by using DMPO as spin trapping agents in q800/PAA systems. (D) EPR signals in different systems by using TEMP as spin trapping agents in q800/PAA system. Experimental conditions (for A and B): $[q800]_0 = 1$ g/L, $[h400]_0 = 2$ g/L, $[PAA]_0 = 2$ mmol/L, $[SMX]_0 = 20$ μmol/L, $[MeOH]_0 = [TBA]_0 = [NaN_3]_0 = 50$ mmol/L, $pH_i = 7.0$, and $T = 25 \pm 2$ °C.

The negligible generation of radicals and $^1O_2$ in the CMR-BCs/PAA system reminded us of the role of the DET mechanism. Dou *et al.* [40] reported an electron-transfer-dominated non-radical mechanism in biochar-activated peroxydisulfate (PDS) systems, where the formation of surface-confined PDS* interfacial complexes was responsible for contaminant degradation. The electron-transfer process in this study was verified by *in-situ* electrochemical analysis. Specifically, the current-time (*I-t*) curves indicates that a dramatic current change appeared with the injection of PAA, attributing to the electron transfer from the q800 sample to PAA for producing metastable interfacial complexes (CMR-BCs-PAA*) (Fig. 4A) [41–43]. However, a subsequent current decrease occurred after the addition of SMX, ascribed to the external electron transfer from SMX to CMR-BCs-PAA* [41]. Further, *in-situ* chronopotentiometry (CP) experiments were conducted to monitor the open-circuit potential (OCP) during the degradation process. As illustrated in Fig. 4B, it is rational that the addition of PAA induced an increase

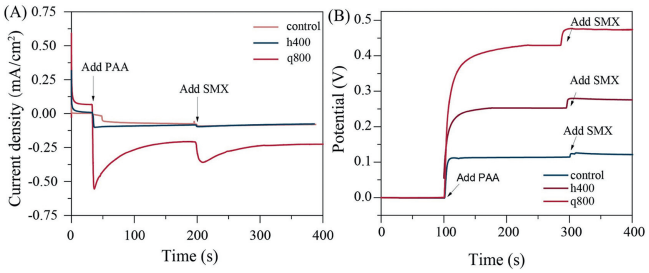
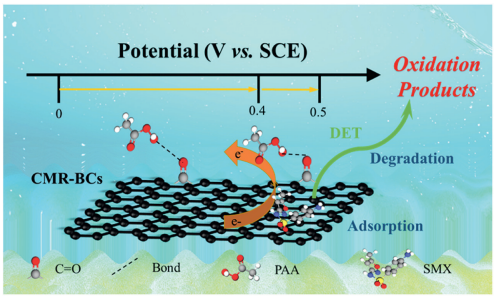


Fig. 4. (A) *I-t* curves and (B) OCP curves in q800/PAA and h400/PAA systems.



Scheme 1. Proposed mechanism of SMX degradation in CMR-BCs/PAA system.

in the potential of the whole system due to the strong oxidation capacity of PAA. The presence of CMR-BC-loaded electrode would further improve the redox potential of the system when PAA was added, indicating the formation of interfacial complexes (CMR-BCs-PAA*) with higher redox potential. Interestingly, the addition of SMX at around 300 s would further induce the increase of redox potential. This increase may be ascribed to the combination of SMX and CMR-BCs-PAA*, which further facilitates the redox cycle from the target contaminant to the interfacial complexes.

Taken together, according to the chemical scavenging tests, EPR analysis, and *in situ* electrochemical tests, the mediated direct electron-transfer mechanism might be responsible for the SMX oxidation in q800/PAA and h400/PAA system. As illustrated in Scheme 1, the interaction between PAA and CMR-BCs induced the formation of interfacial complexes (CMR-BCs-PAA*), which have a higher redox potential (~0.4 V, *vs.* Ag/AgCl) compared to PAA alone (~0.1 V, *vs.* Ag/AgCl). Therefore, the CMR-BCs-PAA* complexes with high redox potential intended to acquire electrons from SMX *via* DET process to achieve SMX degradation [44]. Notably, SMX could further enhance the redox potential of interfacial complexes. Therefore, an internal electron-transfer pathway of SMX-biochar-PAA was formed, facilitating the redox cycle process [45,46].

CMR is a valuable biomass resource, and its recycling to address antibiotic pollution holds environmental implications. In this study, CMR from different prescriptions were pyrolyzed to acquire biochars, which can activate PAA for efficient SMX removal. For the adsorption removal of SMX, the q800 sample exhibited the highest adsorption capacity, attributing to its treated temperature and unique prescription. During the degradation process, the CMR-BCs-PAA* interfacial complexes with enhanced redox potential formed initially, then the presence of SMX further increased the redox potential of the whole system, thereby achieving SMX degradation *via* DET processes. This study proposed using medicinal prescriptions as a classification basis for preparing CMR-BCs, providing a reliable method for recovery and utilization of CMRs. Overall, the findings provide an efficient and green method for resourcing CMR waste and purifying organic wastewater simultaneously.

Declaration of competing interest

The authors declare that they have no known competing financial interests or personal relationships that could have appeared to influence the work reported in this paper.

CRediT authorship contribution statement

Chenghuan Qiao: Writing – review & editing, Writing – original draft. **Yaohua Wu:** Writing – review & editing, Writing – original draft. **Yihong Chen:** Investigation, Visualization. **Chuchu Chen:** Formal analysis, Visualization. **Juanshan Du:** Writing – review & editing, Data curation. **Wenrui Jia:** Data curation. **Yongqi Liang:** Formal analysis. **Qinglian Wu:** Validation, Resources. **Huazhe Wang:** Project administration, Methodology, Funding acquisition. **Wan-Qian Guo:** Project administration.

Acknowledgments

The authors gratefully acknowledge the financial support provided by the National Natural Science Foundation of China (No. 52200049), the China Postdoctoral Science Foundation (No. 2022TQ0089), the Heilongjiang Province Postdoctoral Science Foundation (No. LBH-Z22181), the State Key Laboratory of Urban Water Resource and Environment (Harbin Institute of Technology) (No. 2024TS28), and the Fundamental Research Funds for the Central Universities.

Supplementary materials

Supplementary material associated with this article can be found, in the online version, at doi:10.1016/j.cclet.2025.111526.

References

[1] Z. Wu, Z. Xiong, B. Huang, et al., Nat. Commun. 15 (2024) 7775.
[2] K. Zhang, X. Zhou, P. Du, et al., Water. Res. 123 (2017) 153–161.
[3] H.-C. Luo, W.-Q. Guo, Q. Zhao, et al., Chin. Chem. Lett. 33 (2022) 1293–1297.
[4] A. Abdallah, P. Zhang, Q. Zhong, et al., Curr. Drug Metab. 20 (2019) 54–64.
[5] B. Liu, W. Guo, W. Jia, et al., Environ. Sci. Technol. 55 (2021) 12640–12651.
[6] T. Zhang, T. Wang, B. Mejia-Tickner, et al., Environ. Sci. Technol. 54 (2020) 9652–9661.
[7] X. Ao, W. Wang, W. Sun, et al., Water. Res. 203 (2021) 117458.
[8] Z. Zhao, X. Li, H. Li, et al., ACS ES&T Eng 1 (2021) 1432–1440.
[9] F. Zhou, C. Lu, Y. Yao, et al., Chem. Eng. J. 281 (2015) 953–960.
[10] B. Huang, Z. Wu, H. Zhou, et al., Appl. Catal. B: Environ. Energy 355 (2024) 124157.
[11] K. Luo, Y. Shi, R. Huang, et al., J. Hazard. Mater. 457 (2023) 131790.
[12] H. Wang, C. Qiao, C. Chen, et al., Chin. Chem. Lett. 36 (2025) 110244.
[13] C. Dai, S. Li, Y. Duan, et al., Water. Res. 216 (2022) 118347.
[14] D. Kong, Y. Zhao, X. Fan, et al., Environ. Sci. Technol. 56 (2022) 11707–11717.
[15] Z. Zhou, Y. Yang, G. Xue, et al., Chem. Eng. J. 480 (2024) 148048.
[16] Y. Xue, M. Kamali, T.M. Aminabhavi, et al., Chem. Eng. J. 491 (2024) 152037.
[17] Z. Liu, Z. Wang, S. Tang, et al., Resour. Conserv. Recy. 168 (2021) 105254.
[18] F. Meng, T. Chen, D. Ma, et al., Mediators. Inflamm. 2017 (2017) 4265898.
[19] C. Xu, Y. Wang, C. Zhang, et al., Bioresour. Technol. 391 (2024) 129990.
[20] K. Niu, H. Wang, S.K. Kim, et al., J. Sci. Food Agric. 104 (2024) 1166–1177.
[21] H.Y. Yang, L. Han, Y.Q. Lin, et al., Am. J. Chin. Med. 51 (2023) 1105–1126.
[22] J. Yuan, C. Wang, Z. Tang, et al., Arab. J. Chem. 17 (2024) 105606.
[23] H. Huang, J. Tang, K. Gao, et al., RSC. Adv. 7 (2017) 14640–14648.
[24] W. Jia, H. Wang, Q. Wu, et al., Sci. Total Environ. 880 (2023) 163054.
[25] F. Yang, Z. He, F. Yu, et al., Sci. Total Environ. 867 (2023) 161425.
[26] M. Zheng, S. Zhong, K. Li, et al., Energy Fuels 31 (2017) 13842–13851.
[27] M. Makowska, K. Dziosa, Environ. Technol. Innovation 35 (2024) 103667.
[28] H. Wang, W. Guo, B. Liu, et al., Appl. Catal. B: Environ Energy 279 (2020) 119361.
[29] S. Cui, J. Lv, R. Hough, et al., Environ. Res. 258 (2024) 119444.
[30] L. Liu, G. Deng, X. Shi, Sci. Rep. 10 (2020) 5149.
[31] H. Mittal, A. Al Alili, S.M. Alhassan, Micropor. Mesopor. Mater. 299 (2020) 110106.
[32] M. Keiluweit, P.S. Nico, M.G. Johnson, et al., Environ. Sci. Technol. 44 (2010) 1247–1253.
[33] X. Liu, Z. Hao, C. Fang, et al., Chem. Sci. 15 (2023) 204–212.
[34] W. Wang, J. Lin, S. Shao, et al., J. Environ. Chem. Eng. 11 (2023) 109002.
[35] Q. Wu, Y. Zhang, H. Meng, et al., Chemosphere 357 (2024) 141858.
[36] B. Huang, X. Ren, J. Zhao, et al., Environ. Sci. Technol. 57 (2023) 14071–14081.

[37] Z. Wu, B. Huang, X. Wang, et al., Environ. Sci. Technol. 57 (2023) 14046–14057.
[38] X. Cheng, H. Guo, W. Li, et al., Chem. Eng. J. 396 (2020) 125107.
[39] S. Sanguanmith, J. Meesungnoen, C.R. Stuart, et al., RSC Adv. 8 (2018) 2449–2458.
[40] J. Dou, Y. Tang, Z. Lu, et al., Environ. Sci. Technol. 57 (2023) 5703–5713.
[41] Y. Zhao, H. Dai, J. Ji, et al., Sep. Purif. Technol. 288 (2022) 120650.
[42] M. He, P. Zhao, R. Duan, et al., J. Hazard. Mater. 424 (2022) 127568.
[43] S. Liu, J. Du, H. Wang, et al., Water Res. 254 (2024) 121417.
[44] L. Meng, C. Zhao, H. Chu, et al., Chin. J. Catal. 59 (2024) 346–359.
[45] Y. Wu, H. Wang, J. Du, et al., Environ. Sci. Technol. 57 (2023) 16662–16672.
[46] C. Yu, Z. Wu, H. Shi, et al., Chin. Chem. Lett. 35 (2024) 109334.